Journal of Science and Technology in Civil Engineering, HUCE (NUCE), 2022, 16 (3): 29–45

DISTINGUISHED PUNCHING SHEAR BEHAVIOUR OF UNBONDED POST-TENSIONED CONCRETE SLAB – CFT COLUMN VS REINFORCED CONCRETE SLAB – CFT COLUMN CONNECTIONS

Binh Luu-Thanh[a,b], Long Nguyen-Minh[a,b], Takayuki Namba[c], Kei Nakagawa[d],

Koji Oki[e], Cuong Ngo-Huu[a,b,*]

[a]*Faculty of Civil Engineering, Ho Chi Minh City University of Technology (HCMUT), 268 Ly Thuong Kiet Street, District 10, Ho Chi Minh City, Vietnam*
[b]*Vietnam National University Ho Chi Minh City, Linh Trung Ward, Thu Duc City, Ho Chi Minh City, Vietnam*
[c]*Civil & Infrastructure Engineering Research Department, JFE Steel Corporation, Japan*
[d]*Planning & Marketing Department, JFE Steel Corporation, Japan*
[e]*Construction Materials Engineering Department, JFE Steel Corporation, Japan*

Article history:
Received 18/5/2022, Revised 10/6/2022, Accepted 13/6/2022

Abstract

This article evaluates and compares the punching shear behaviour of unbonded prestressed concrete (UPC) slab - concrete-filled steel tube (CFT) column connections/joints with that of reinforced concrete (RC) slab – CFT column connections. The experimental program was carried out on five large-sized samples, including three UPC slab - CFT column samples and two RC slab - CFT column samples. Steel plate connection details were utilised to increase the bond between the concrete slab and the CFT column. The experimental results showed that the prestressing tendons significantly increased the pre and post-cracking stiffness of the slab-column connections, thereby, greatly reducing the deflection of the UPC slab - CFT column samples than that of the RC slab - CFT column samples, especially during the serviceability phase (by up to 58%). However, the use of tendons resulted in a significant decrease in the ductility and energy absorption index of the UPC slab - CFT column samples compared to that of the RC slab - CFT column samples (by up to 44% and 41%, respectively). Using prestressing tendons slightly increased the punching shear capacity, and significantly reduced the strain of the connection details such as the vertical ribs and the horizontal bearing plate. At the same time, the tendons helped greatly reduce the strain of the longitudinal rebars in the UPC slabs.

Keywords: unbonded post-tensioned concrete (UPC); connection/joint; CFT column; flat slab; connection details; punching shear; experiment.

https://doi.org/10.31814/stce.huce(nuce)2022-16(3)-03

1. Introduction

The structure comprising reinforced concrete (RC) flat slab and concrete-filled steel tube (CFT) column is considered structurally and economically efficient due to its high load-bearing capacity, ductility and energy absorption capacity, and reduced construction cost and time [1–5]. However,

*Corresponding author. *E-mail address:* ngohuucuong@hcmut.edu.vn (Ngo-Huu, C.)

the application of the RC slab – CFT column connection/joint is limited in the situation where large space and spans are required. A viable solution to this problem is to use prestressed concrete (PC) slab - CFT column connection. The structure is called an unbonded or bonded prestressed concrete (UPC or BPC) structure if the prestressing tendon is unbonded or bonded, respectively. In comparison with bonded tendons, using unbonded tendons can offer reduced construction costs [6], which results in many applications of the UPC structure [2, 7–10]. However, owing to a lack of the tendon strain compatibility with adjacent concrete and the prestressing forces being only transmitted to the UPC structure at the anchorages [6, 11, 12], the analysis of the UPC structure is more complex than the BPC counterpart.

In the structural aspect, both RC slab – CFT column and PC slab – CFT column connections face the problem of brittle punching shear failure because of stress concentration at the slab – CFT column joint [2, 3, 13]. In addition, the non-monolithic characteristic of the connection between flat slabs and CFT columns can significantly affect the structural integrity and the punching shear behaviour of the flat slab – CFT column connection [14]. The punching shear response of RC slab – CFT column connections has been well investigated in many studies [1, 4, 5, 14–22]; however, the research effort toward PC slab - CFT column connections is still very limited [7]. It is noteworthy that the prestressing force can embrittle the behaviour and reduce the ductility and energy absorption capacity of PC members [12, 23–25]. Therefore, the punching shear performance of the PC slab – CFT column connection, especially the difference in the structural response with the RC slab – CFT column connection, deserves careful investigation.

This study aims to experimentally investigate the punching shear behaviour of RC/UPC slab - CFT column joints using steel plate connections. The test program was conducted on five large-scale flat slab - CFT column samples. Among these samples, there were three UPC slab - CFT column connections and two RC slab - CFT column connections. The main goal of this study is to quantify and compare the punching shear resistance, deformation, ductility and energy absorption capacity of these flat slab - CFT column connections.

2. Experimental program

2.1. Material properties

In this study, the concrete mix design consisted of Portland cement PC40 (460 kg/m^3), 20-22 mm coarse aggregates (1048 kg/m^3), 2-4 mm river sand (640 kg/m^3) and clean water (194 l/m^3). The slump of the concrete 12 ± 2 cm, which is a typical range for casting structural members [23, 24, 26]. The compressive strength of concrete (f_c) was derived from the mean values of three 150×300 mm concrete cylinders according to TCVN 10303:2014 [27]. The mechanical properties of the steel reinforcement and steel plates were determined as per TCVN 197-1:2014 [28]. Table 1 summaries the mechanical properties of the materials used in this study in which $f_{sr,y}$ and $f_{sr,u}$ are the yield and ultimate strength of the longitudinal reinforcement of the slab, respectively; $f_{stu,y}$ and $f_{stu,u}$ are respectively the yield and ultimate strength of the steel tube; $f_{svr,y}$ and $f_{sh,y}$ are respectively the yield strength of the vertical rib plates and horizontal bearing plates; $f_{svr,u}$ and $f_{sh,u}$ are respectively the ultimate strength of the vertical rib plates and horizontal bearing plates; and f_{py} and f_{pu} are the nominal yield and ultimate strength of the prestressing tendons, respectively. Young's modulus of the tendon (E_p) was 196 GPa.

Table 1. Mechanical properties of the materials (MPa)

Sample	f_c	$f_{sr,y}$	$f_{sr,u}$	$f_{stu,y}$	$f_{stu,u}$	$f_{svr,y}$	$f_{sh,y}$	$f_{svr,u}$	$f_{sh,u}$	f_{py}	f_{pu}
SP-T1-16 SP-T3-16a SP-T3-16b	40.4	420	594	324	428	331	372	478	513	1666	1851
S-T1-16 S-T3-16a		420	594	324	428	331	372	478	513	-	-

2.2. *Experimental samples*

The experimental samples consisted of five flat slab-column connections with width × breath × thickness = 2500 × 2500 × 200 mm (Fig. 1). The CFT column had a circular cross-section with a diameter of 400 mm, a height of 1300 mm and a thickness of the steel tube of 9 mm. Table 2 tabulates the experimental parameters of this study.

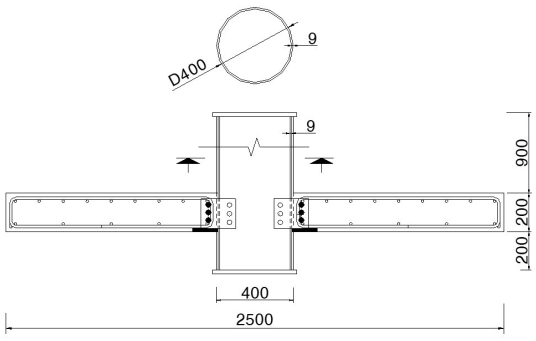

Figure 1. A typical cross-section of the test sample

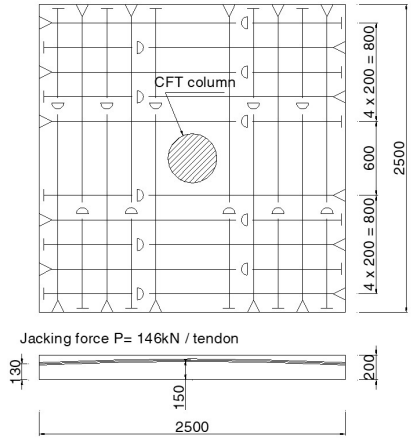

Figure 2. Arrangement of the tendons in the UPC slab (dimensions in mm)

The UPC slabs were post-tensioned with unbonded 7-wire strands with a nomial diameter of 12.7 mm (Fig. 2). The UPC slabs were designed with Class U (uncracked) as per ACI 318-19 [29]. The initial jacking force P_i = 146 kN per tendon. The camber of the UPC samples due to the post-tensioning was from 0.211-0.275 mm. The diameter of both the tensile and compressive reinforcement of the slabs was 14 mm. The respective reinforcement ratio of ρ_{st} = 0.77% and ρ_{sc} = 0.39%. The arrangement of the reinforcement is shown in Fig. 3.

Two different kinds of connection details (T1 and T3) between the CFT column and the flat slab were proposed in this study and displayed in Fig. 4. It is worth noting that the same welding material and technique (angle welding) with a welding height of 8 mm were used to make all the test samples.

Firstly, connection detail T1 (Fig. 4(a)) was comprised of annular horizontal bearing plates and vertical ribs. The internal and external diameters of the horizontal bearing plate were respectively D_i = 400 mm and D_o = 650 mm. The thickness of the horizontal bearing plate was 16 mm. The horizontal bearing plate was fully welded to the steel tube. The bottom level of the horizontal bearing

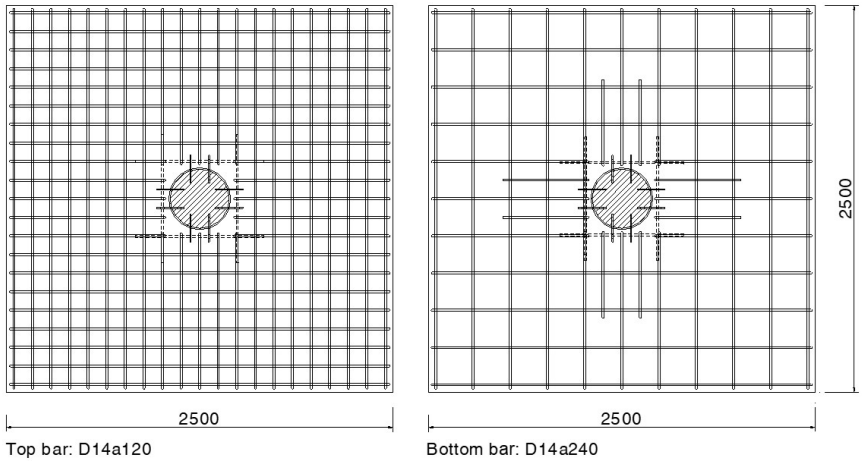

Figure 3. Arrangement of the reinforcement in the slab (dimensions in mm)

plate was aligned with the slab's bottom surface to expedite the erection of formwork and to enhance the vertical rib's resistance against fire. Regarding the vertical rib, it consisted of four pairs with a distance between the ribs in each pair of 120 mm (Fig. 4). The cross-section of the vertical rib was rectangular with the dimension $b_v \times h_v \times t_v = 180 \times 155 \times 8$ mm (Fig. 4(c)). The connection between the vertical ribs with the steel tube and the horizontal bearing plate was full penetration welding. The vertical ribs were also arranged inside the CFT column to enhance the bonding between the steel tube with the enclosed concrete, which could help avert the potential splitting between these two constituents because of the negative moment at the connection. The vertical ribs outside the column had the width $b_{v,o} = 98$ mm and were drilled with three holes of 25 mm in diameter. In each hole, there was a rebar of 14 mm in diameter passing through to increase the dowel action. The vertical ribs inside the column had the width $b_{v,i} = 73$ mm and three holes of 25 mm in diameter. Connection detail T1 was used for samples SP-T1-16 and S-T1-16. Secondly, connection detail T3 (Fig. 4(b)) had four rectangular horizontal bearing plates with 16 mm in thickness instead of using annular plates as T1 to decrease material and simplify the installation. The dimension of these rectangular horizontal

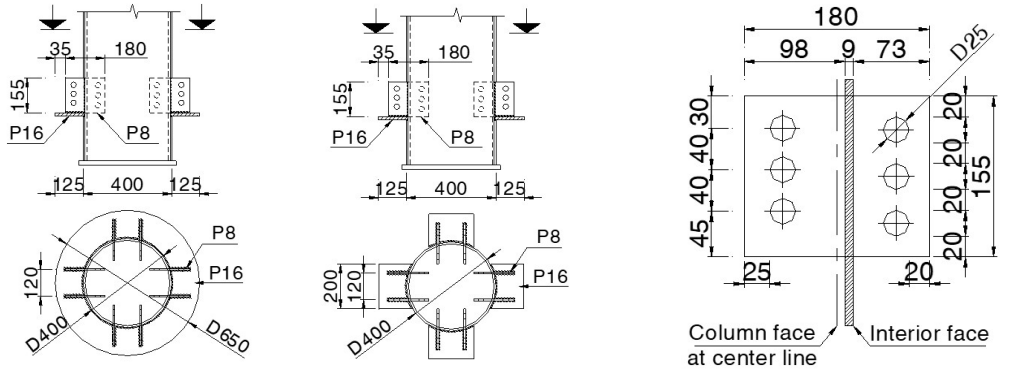

(a) T1 (b) T3 (c) Vertical ribs (dimensions in mm)

Figure 4. Connection details

bearing plates was $b_h \times l_h \times t_h = 200 \times 125 \times 16$ mm. The horizontal plates were welded to the steel tube. The samples using T3 were SP-T3-16a, SP-T3-16b and S-T3-16a.

It is noteworthy that in comparison with the common use of steel profile (I or H – shape) for the connection details, the use of steel plates gives more advantages in terms of construction time and costs because the size and weight of the steel plate are significantly smaller than that of the steel profile. In addition, connection details involving steel plates help soften the stiffness of slab - CFT column connections; therefore, it can significantly reduce the stress concentration at the joint, thereby limiting the possibility of a punching shear failure.

Table 2. Test parameters

Sample	Dimension (m)	Type of Connection detail	Thickness of steel tube	Horizontal bearing plate				Vertical rib						Rebar ratio	
			t (mm)	Shape	D_o (b_h) (mm)	D_i (l_h) (mm)	t_h (mm)	Shape	b_v (mm)	h_v (mm)	t_v (mm)	$b_{v,o}$ (mm)	$b_{v,i}$ (mm)	$\rho_{s,t}$ (%)	$\rho_{s,c}$ (%)
SP-T1-16	2.5 × 0.2	T1	9	AN	650	400	16	REC	180	155	8	98	73	0.77	0.385
SP-T3-16a		T3		REC	200	150	16								
SP-T3-16b		T3		REC	200	150	16								
S-T1-16		T1	9	AN	650	400	16	REC	180	155	8	98	73	0.77	0.385
S-T3-16a		T3		REC	200	150	16								

In Table 2, AN is Annular; REC is Rectangular; b_h and l_h are respectively the width and length of the rectangular horizontal bearing plate; b_v, h_v, and t_v are respectively the width, height, and thickness of the vertical rib; $b_{v,o}$ and $b_{v,i}$ are respectively the width of the vertical rib outside and inside the steel tube; D_o and D_i are respectively internal and external of the annular horizontal bearing plate; t is the thickness of the steel tube; t_h is the thickness of the horizontal bearing plate; ρ_{st} and ρ_{sc} are respectively the tensile and compressive reinforcement ratio.

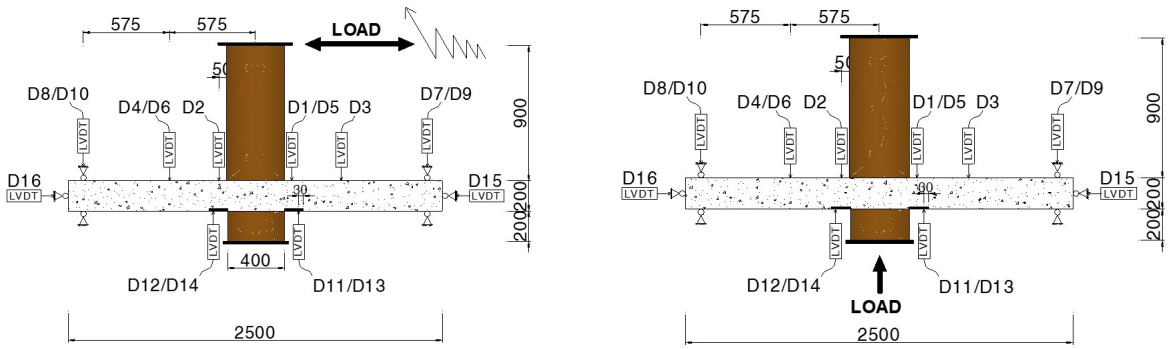

(a) Phase 1 – Lateral loading

(b) Phase 2 – Vertical loading

Figure 5. Loading method and instrumentation

The samples were tested using the simply supported condition as illustrated in Fig. 5. The vertical deflection of the sample was monitored via 14 linear variable differential transducers (LVDTs). Of them, LVDTs D1 - D10 were for measuring the vertical deflection at the midspan, quarter-span and edge of the slabs. LVDTs D11 - D14 at the outer edge of the horizontal plates were used for the

samples with the CFT column. Besides, the lateral deflection of the samples was measured by two LVDTs (D15 and D16) arranged at the sides of the slab.

The strain of the horizontal bearing plates, vertical ribs, concrete and longitudinal rebars were recorded through 17 strain gauges (SGs). Among those SGs, six SGs P1-P6 were to measure the strain of the horizontal bearing plates and vertical ribs as shown in Fig. 6(a). The strain of the tensile rebars was measured by six SGs S1-S6 bonded to four rebars at the upper layer in two directions through the column centre (80 mm and 280 mm away from the surface of the column, respectively) as exhibited in Fig. 6(b). The compressive strain of concrete was recorded via five SGs C1 - C5.

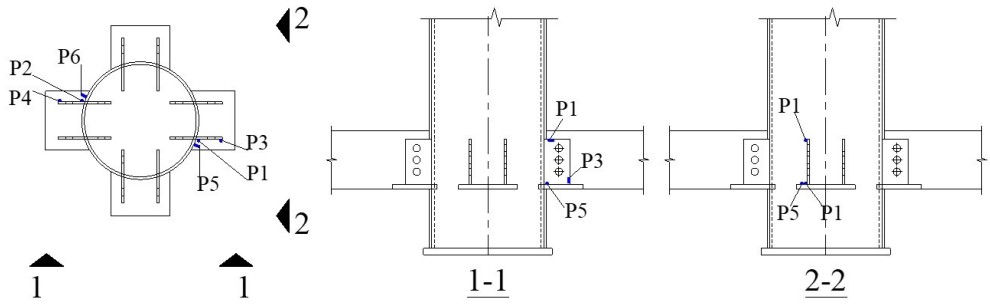

(a) The horizontal bearing plates and vertical ribs

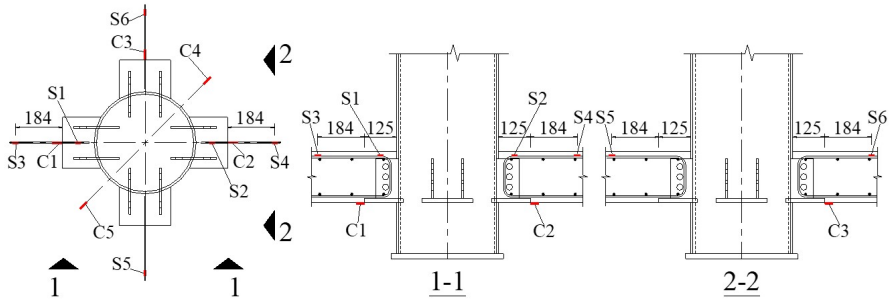

(b) The concrete and rebars

Figure 6. Layout of strain gauges (SGs)

The loading method encompassed two phases, i.e. Phase 1 – lateral loading and Phase 2 – vertical loading. In Phase 1, the sample was loaded by five lateral quasi-static loading cycles to simulate the immediate occupancy as per ACI PRC-374.2-13 [30] with a constant amplitude of the lateral deflection = 0.5% drift according to ACI 318-19 [29] (Fig. 5(a)). This loading phase is intended to cause a certain impact of lateral loads on the response of the connecting constituents (e.g. the horizontal bearing plates and vertical ribs) and in turn the punching shear capacity of the slab – CFT column connections. The lateral loading was removed completely after Phase 1. In Phase 2, the sample was subjected to vertical loads to collapse by using a hydraulic jack with a capacity of 500 tons. It was observed in the previous experimental investigations [25, 31, 32] that a loading rate of 15-30 kN/min could simulate quasi-static loading and the load-bearing resistance of the samples in those studies was similar compared to the samples in this study. This loading rate of 15-30 kN/min was, therefore, selected in this study (Fig. 5(b)). During the experiment, the data of the applied loads, deflection and strain of the sample was automatically monitored by a data acquisition system. Fig. 7 shows the sample before casting while Fig. 8 shows the test setup.

Figure 7. Unbonded prestressed concrete slab before casting

Figure 8. Test setup of the sample

3. Experimental results and discussion

3.1. Failure pattern

Table 3 summarises the test results of the samples. The test results showed that the lateral loads in Phase 1 did not create any crack in the UPC slab – CFT columns connections. In Phase 2 of vertical loading, all the samples collapsed in a punching shear manner as shown in Fig. 9. For the RC slab – CFT column specimens, the first radial cracks appeared at 24.5-27% of $V_{u,CFT}$ ($V_{u,CFT}$ is the maximum applied load). Meanwhile, owing to the effect of prestressing, the corresponding value (30.2-37.2% of $V_{u,CFT}$) for the UPC slab – CFT column samples was higher with smaller crack width. Increasing the applied loads caused other radial cracks to appear. The radial cracks were quite uniformly distributed (Fig. 9). Tangential cracks also occurred and grew when the load increased, which resulted in the formation of a punching shear cone and the collapse of the samples (Fig. 9). The failure of the slab–column connections was sudden with a loud bang. Cross-section at central line of the tested slab – CFT column connections are shown in Fig. 10.

In Table 3, V_{cr}, V_y and V_u are respectively the cracking, yielding and maximum load; δ_{cr}, δ_y and δ_u are respectively the vertical displacements of the slab at the cracking, yielding and ultimate load; α is the inclination angle of the punching shear cone; $\varepsilon_{ribu,h}$ and $\varepsilon_{ribu,v}$ are respectively the maximum strain in the horizontal bearing plate and the vertical rib; $\varepsilon_{su,reb}$ and ε_{cu} are respectively the maximum tensile strain of rebars and maximum compressive strain of concrete; K_1 and K_2 are respectively the secant stiffness of the specimen in the pre-cracking and post-cracking phase (Fig. 13); A_1, A_2 are respectively

energy absorption in the pre-yielding and post-yielding phase (Fig. 16); *EAI* is the energy absorption index, $EAI = [(A_1 + A_2)/A_1]$.

Table 3. Test results

Specimens	V_{cr} (kN)	V_y (kN)	V_u (kN)	δ_{cr} (mm)	δ_y (mm)	δ_u (mm)	α (degree)	μ	$\varepsilon_{ribu,h}$ (‰)	$\varepsilon_{ribu,v}$ (‰)	$\varepsilon_{su,reb}$ (‰)	ε_{cu} (‰)	ε_{pu} (‰)	K_1 (kN/mm)	K_2 (kN/mm)	A_1 (kNmm)	A_2 (kNmm)	*EAI*
SP-T1-16	363	528	974	1.32	3.06	17.88	21.1	5.84	0.40	3.25	1.72	1.5	1.5	43.3	14.9	190	1805	10.5
SP-T3-16a	310	523	993	1.21	3.92	22.20	20.6	5.66	0.18	4.32	1.23	2.1	1.6	40.4	12.3	235	2305	10.8
SP-T3-16b	288	525	955	1.11	3.68	18.66	20.4	5.07	0.17	4.97	2.08	1.7	1.5	40.9	14.5	191	1825	10.6
S-T1-16	231	383	943	0.88	3.85	32.37	20.9	8.41	1.9	8.0	2.2	1.1		41.3	8.1	208	3329	17
S-T3-16a	249	384	921	1.01	4.23	38.41	19.1	9.08	1.0	5.4	2.7	0.8		38.8	6.6	237	4031	18

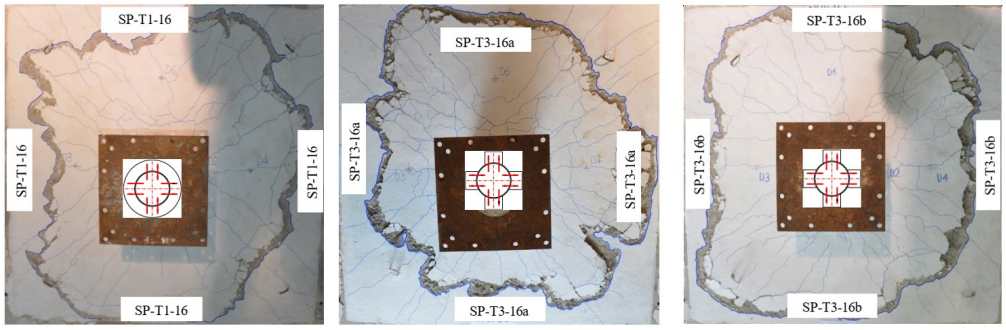

(a) UPC slab – CFT column connections

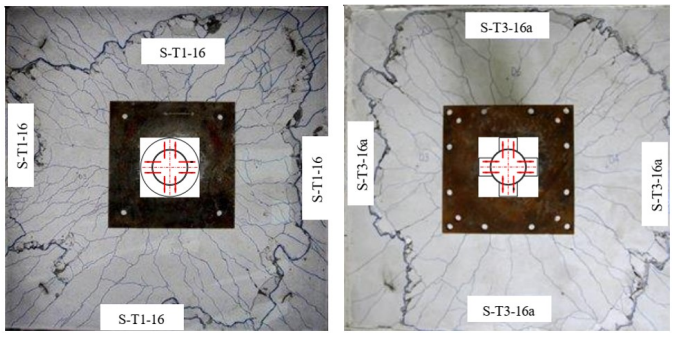

(b) RC slab – CFT column connections

Figure 9. Punching cone shape at the top face of the slab

At the top face of the slab (see Figs. 9 and 10), the average of eight distances (see Figs. 11) between the edge of the punching cone and the outer surface of the CFT column r_{ave} was 4.3 – 4.7d (d is the effective thickness of the slab) for the UPC slab – CFT column samples. The corresponding value rave for the RC slab – CFT column connections was 4.7 – 4.9d. The inclination angle of the punching cone α_{ave} is the average of four angles as shown in Fig. 11. The inclination angle α_{ave} of the UPC slab – CFT column samples was 20.4°-21.1°. The corresponding value α_{ave} for the two RC slab – CFT column samples was 19.1°-20.9°. The shape of the horizontal bearing plates (one annular plate connection T1 or four rectangular plates connection T3) was found to have an insignificant effect on the shape and inclination angle of the punching shear cone.

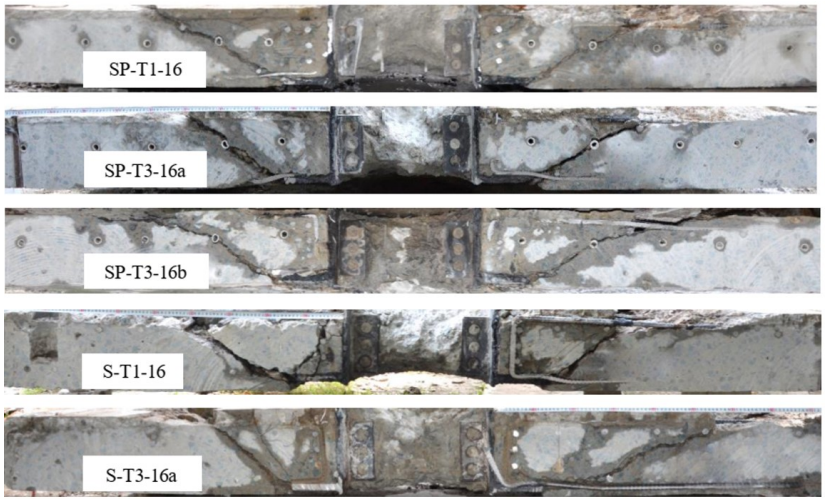

Figure 10. Typical cross-section of the tested slab – CFT column connections

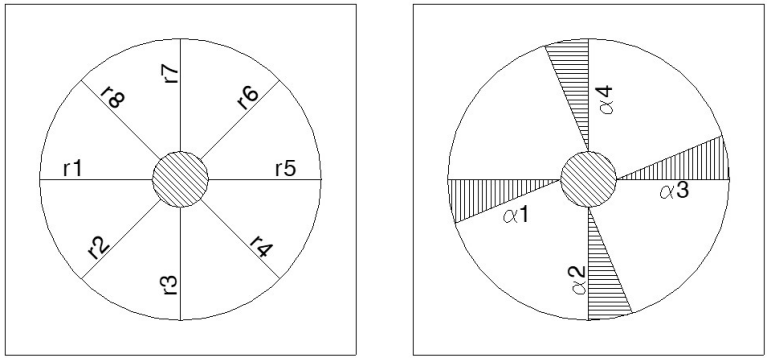

Figure 11. Obtained distances and angles of the punching cone

3.2. Load-deflection relationship

Fig. 12 displays the relation between the applied load and deflection of the samples. The load-deflection relationship of the samples could be divided into two phases: the phase before cracking (elastic phase) and the phase after cracking to the failure of the samples (post-cracking phase). The load level corresponding to the appearance of the first crack was called the cracking load V_{cr}. The cracking loads of the UPC slab – CFT column and the RC slab – CFT column samples were respectively $V_{cr} = 37.2\%V_u$ and $V_{cr} = 27\%V_u$ with V_u = the maximum load.

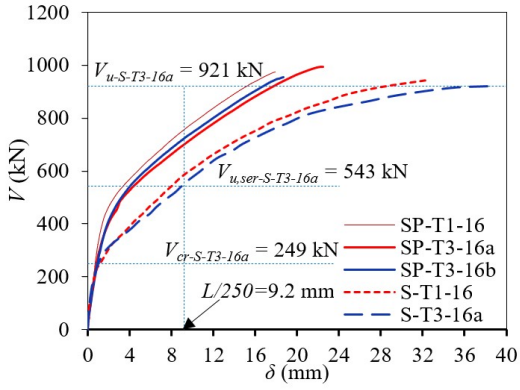

Figure 12. Load-deflection of the test samples

In the first elastic phase, the relationship of load-deflection of the samples was linear and similar to each other. This means that both the pre-stressing tendon and connection details (T1 and T3) did not play a significant role in the performance

of the flat slab–column connections during the elastic phase.

In the post-craking phase from V_{cr} to V_u, the behaviour of the samples changed to nonlinearity and the difference in behaviour between the samples became pronounced. During this phase, the appearance and development of cracks reduced the stiffness and consequently increased the ultimate deflection of the samples significantly. Compared to the RC slab sample, the prestressing tendons in the UPC slab sample enhanced its stiffness and in turn reduced its deflection. For instance, at the serviceability limit load $V_{u,ser}$ (the load causing the vertical deflection of the sample = L/250 = 2300/250 = 9.2 mm with L = the span) of the RC slab – CFT column sample S-T3-16a ($V_{u,ser-S-T3-16a}$= 543 kN), the deflection of the UPC slab – CFT column samples was up to 58% smaller compared to the RC slab – CFT column samples. This observation means that on the one hand, prestressing embrittles the behaviour of the sample but on the other hand, prestressing is effective in controlling the deflection of the samples which is an important design criterion at the serviceability state.

The maximum deflection of the UPC slab samples was smaller than the RC slab sample by 45% for the sample with connection T1 (one continuous annular horizontal plate) and 51% for the sample with connection T3 (four discrete rectangular horizontal plates) (Fig. 13(a)). The change in the shape of the horizontal bearing plate from one continuous annular plate to four discrete rectangular plates did not have a significant effect on the deformation capacity of the slab-column connections.

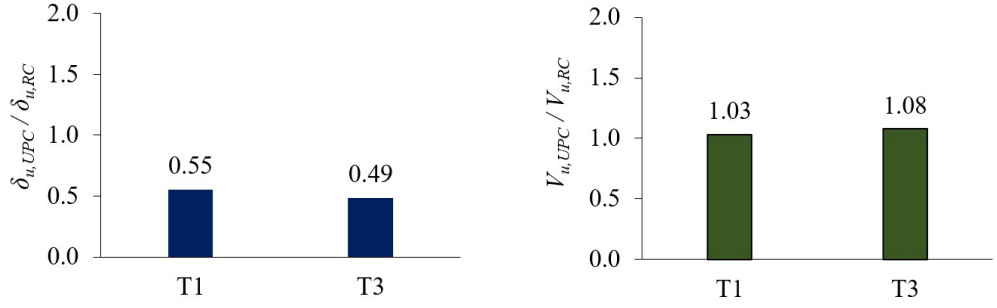

(a) Maximum deflection (b) Maximum vertical load

Figure 13. The Comparison in deflection and load

3.3. Punching shear capacity and stiffness of the slab-column connection

The punching shear capacity of the UPC slab – CFT column samples was 3-8% greater than that of the RC slab – RC column samples (Fig. 13(b)). This means that there was an insignificant contribution of the prestressing tendon to the sample's punching shear capacity. One possible explanation for this phenomenon could be because of the small oblique angle of the tendon in regard to the slab plane at the failure section of the sample (approximately 1°). This led to a negligible vertical force component of the tendon – the main component against the shear forces. Another reason could be that the punching shear capacity of the slabs is largely reliant on the mechanical properties of concrete. In this study, the concrete strength of the UPC and RC slabs was chosen to be the same (to only investigate the effect of the prestressing tendons).

Table 3 shows the values of K_1 and K_2 which are respectively the secant stiffness of the slab–column connections in the elastic phase prior to concrete cracking and post-cracking phase as shown in Fig. 14. The yield point of the sample was computed following the study [33]. In the elastic phase, the elastic stiffness K_1 of the UPC slab – CFT column samples was roughly 5% greater than the RC slab

– CFT column samples. In the post-cracking phase, compared to the RC slab – CFT column samples, thanks to the positive influence of the prestressing, K_2 of the UPC slab – CFT column samples increased by 85% for the sample with the annular horizontal plate and up to 118% for the sample with the rectangular horizontal plates (Fig. 15(a)).

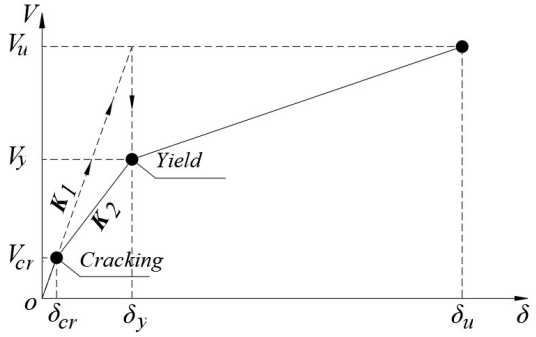

Figure 14. Definition of K_1 and K_2

Notes: K_1 and K_2 are respectively the secant stiffness of the slab-column connections in the elastic phase prior to concrete cracking and post-cracking phase; $K_1 = V_{cr}/\delta_{cr}$ and $K_2 = \left(V_y - V_{cr}\right)/\left(\delta_y - \delta_{cr}\right)$; V_{cr} and V_y (kN) are respectively the cracking and yielding load; δ_{cr} and δ_y (mm) are respectively the deflection of the slab at the cracking and yielding load.

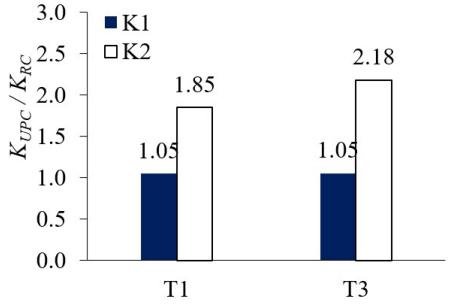

(a) Stiffness K_1 and K_2

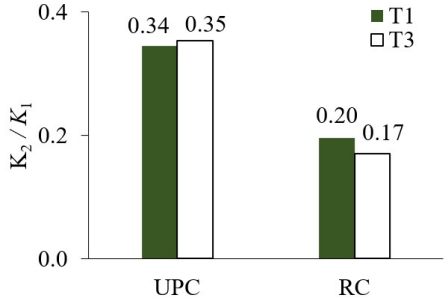

(b) Stiffness deterioration

Figure 15. Stiffness K_1; K_2 and stiffness deterioration in the post-cracking phase

The stiffness deterioration (K_2/K_1) in the post-cracking phase compared to the elastic phase of the samples is shown in Fig. 15(b). It is evident that the prestressing tendons helped reduce the stiffness deterioration of the UPC slab – CFT column samples more than that of the RC slab - CFT column samples. For example, the stiffness deterioration of the former was about 2.1 times smaller compared to the latter as shown in Fig. 15(b).

3.4. Ductility and energy absorption

The ductility index μ of the samples was calculated as the ratio between the deflection of the sample at the yield point (as defined in Fig. 14) and that at failure (δ_y/δ_u) according to the previous studies [6, 9]. The ductility index μ of the test samples is tabulated in Table 3.

In comparison with the RC slab – CFT column sample, μ of the UPC slab – CFT column sample decreased by 31% when using connection T1 (the annular horizontal bearing plate) and by up to 44% when using connection T3 (the rectangular horizontal bearing plates) (Fig. 16(a)). This finding also shows the effect of the horizontal bearing plates on the ductility of the slab – CFT column connections.

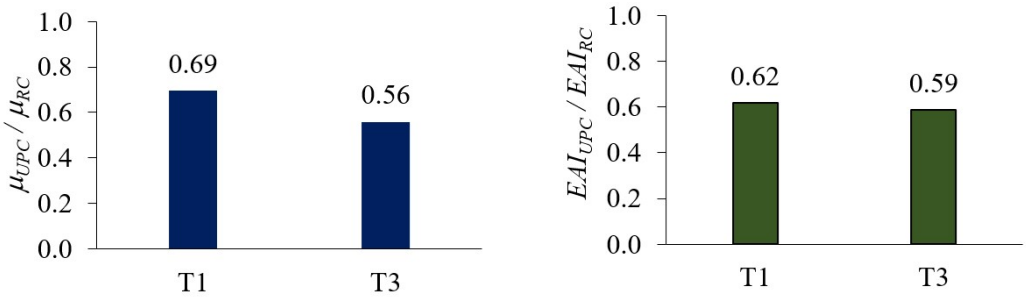

(a) Ductility index (b) Energy absorption index

Figure 16. The comparison in ductility index and energy absorption index

The energy absorption index of the samples in this study was calculated as $EAI = (A_1 + A_2)/A_1$, where A_1 and A_2 are the areas under the load-deflection curve or the energy absorption capacity in the pre and post-yielding phase as illustrated in Fig. 17. The yield point was determined as per [33]. In comparison with the RC slab – CFT column samples, the use of prestressing tendons reduced the EAI of the UPC slab – CFT column samples by 38% when using connection T1 (the annular horizontal plate) and by 41% when using connection T3 (the rectangular horizontal plates) (Table 3). The total energy absorption capacity ($A_1 + A_2$) of the UPC slab – CFT column samples was smaller by 47-56% than that of the RC slab – CFT column samples (Table 3). The UPC slab – CFT column sample with connection T3 had the energy absorption capacity slightly higher than the UPC slab – CFT column sample with connection T1 (by about 3%).

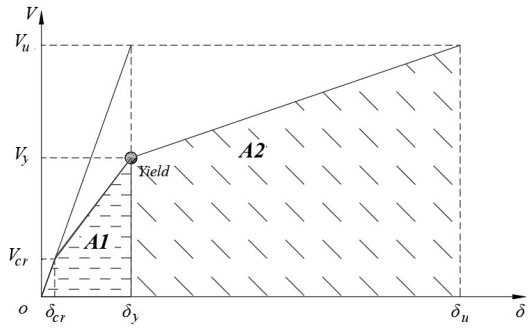

Figure 17. Area A_1 and A_2

3.5. Load-strain of vertical ribs and horizontal bearing plates

The relationship of load-strain of the vertical ribs at the upper and lower corner and the horizontal bearing plates were respectively shown in Figs. 18(a), (b) and (c). The vertical rib was inclined to carry loads earlier than the horizontal bearing plate and its strain growth was considerably influenced by the configuration of the horizontal bearing plate and by the tendons. For instance, at the yielding load of sample S-T3-16a ($V_{y-S-T3-16a}$ = 384 kN), the strain at the vertical rib's upper corner of the UPC slab – CFT column sample with connection T1 was 2.2-5.1 times higher than that of the sample with connection T3. For the RC slab – CFT column samples, the strain at the vertical rib's upper corner of the sample with connection T1 was 88% of that of the sample with connection T3.

The strain of the vertical ribs was ununiformly distributed as displayed in Figs. 18(a) and (b). In the RC slab – CFT column connections, the upper corner of the vertical rib (P1) tended to work earlier than the lower corner (P3) and the P1 strain had a decreasing trend after the appearance of cracks. This finding could be attributed to the fact that the vertical rib's upper corner was near the slab's tension side. Consequently, it early carried the tensile stress transmitted from the slab via the dowel action developed at the holes of the vertical rib. However, for the UPC slab – CFT column connections, the

tendon in the slab's tension side was the main component in resisting the tensile stress in the slab, leading to an insignificant contribution of the vertical rib's upper corner. Therefore, strain P1 was smaller compared to strain P3. After concrete cracking, strain P3 was inclined to develop at a faster speed than strain P1. The strain of the horizontal bearing plates of all the test samples was quite similar and insignificant when compared to the vertical ribs (Fig. 18(c)).

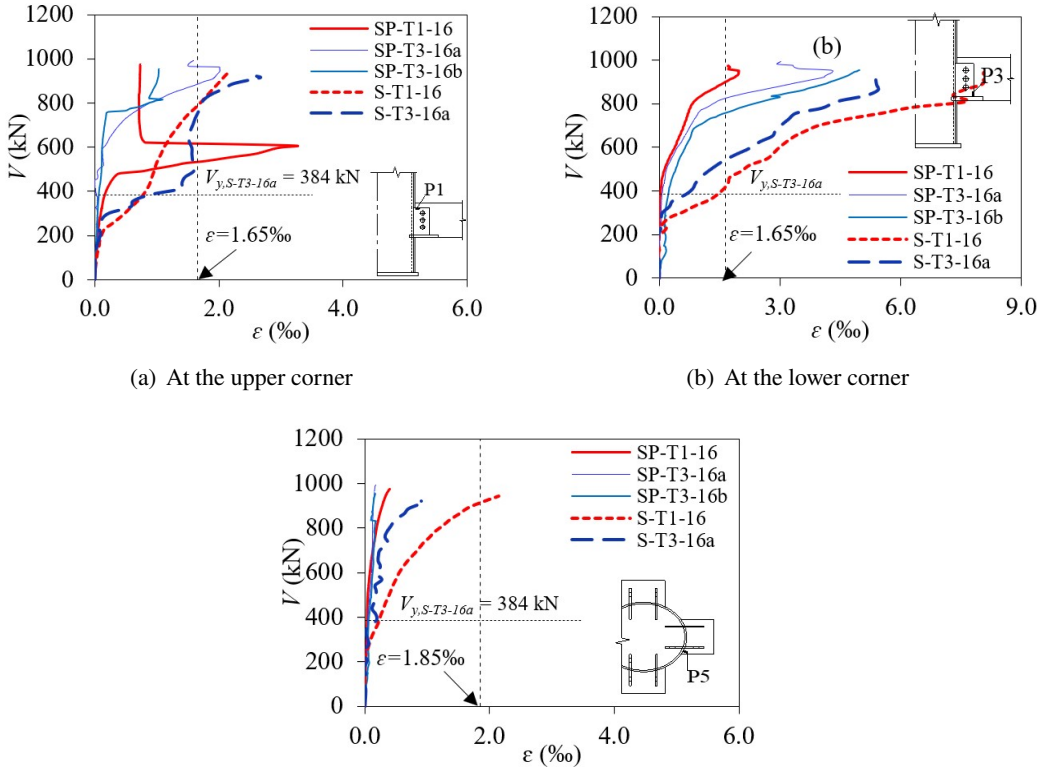

(a) At the upper corner

(b) At the lower corner

(c) Horizontal bearing plates

Figure 18. Load-strain curve of the vertical ribs and the horizontal bearing plates

Changing the configuration of the horizontal bearing plate exerted a pronounced influence on the maximum strain of the vertical rib and the horizontal bearing plate. The maximum strain of the vertical rib at P1 of the UPC – CFT column sample with connection T1 (one continuous annular horizontal bearing plate) was 1.6-3 times greater compared to the sample with connection T3 (four discrete rectangular horizontal bearing plates) (Fig. 18(a)). The maximum strain of the horizontal bearing plate of the sample with connection T3 was about 44% of the sample with connection T1. The use of tendons substantially decreased the maximum strain of the vertical rib and the horizontal bearing plate, for example, by 75-81% in the sample SP-T1-16 compared to sample S-T1-16. At the failure of the sample, the vertical ribs in most of the samples yielded but the horizontal bearing plates had not yielded (Fig. 18).

3.6. Load-strain of concrete, reinforcement and prestressing tendons

The load-strain of the concrete in compression, the rebar and the tendon are shown in Fig. 19.

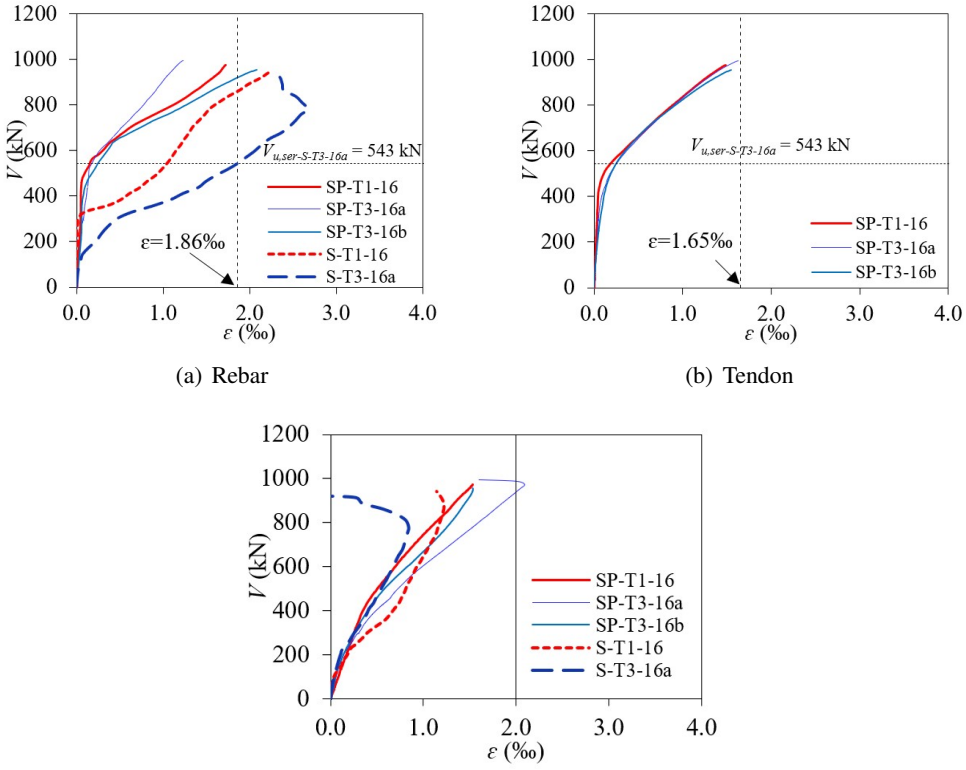

Figure 19. Load-strain curve of rebar, tendon and concrete in compression

The tensile rebars in the RC slab - CFT column samples had a tendency to carry stress earlier and more compared to the UPC slab - CFT column sample as shown in Fig. 19(a). At the serviceability limit load of sample S-T3-16a ($V_{u,ser-S-T3-16a}$ = 543 kN), the prestressing tendons helped reduced the rebar strain by 86% for the sample with connection T1 and by 91% for the sample with connection T3. The maximum rebar strain in the UPC slab - RC column samples with connection T1 and T3 was 1.7‰ and 1.2-2.1%, respectively. Meanwhile, the corresponding value in the RC slab - CFT column samples was 2.2-2.7‰. These results mean that the rebars in the RC slab - RC column samples yielded while most of the rebars in the UPC slab - RC column samples had not yielded.

The strain of the tendons in all the samples was fairly similar indicated in Fig. 19(b). At the failure of the sample, the strain of the tendons was 1.62‰ (Table 3) and thus the tendon had not yielded.

The maximum strain of concrete in the UPC slab – CFT column samples was greater than that of the RC slab – CFT column samples (Fig. 19(c)). The maximum strain of concrete in the UPC slab – CFT column samples was 1.5-2.1‰ (Table 3). The corresponding number in the RC slab – CFT column samples was 0.8-1.1‰. The concrete strain in the UPC slab – CFT column sample with connection T3 was 37% greater than the sample with connection T1, which shows the influence of the configuration of the horizontal bearing plate on the concrete strain. It is noteworthy that the maximum concrete strain in all the samples was less than 2‰ (Table 3).

4. Conclusions

This study experimentally analyses and compares the punching shear behaviour, punching shear resistance, deformation, ductility and energy absorption of the UPC slab - CFT column connections with that of the RC slab - CFT column connections. The experimental program was carried out on five large-scale samples of the slab - CFT column connections/joints, in which, there were three UPC slab - CFT column samples and two RC slab - CFT column samples. Based on the results obtained from this study, some conclusions can be drawn as follows:

(i) In comparison with the RC slab - CFT column samples, the use of prestressing tendons marginally enhanced the punching shear capacity of the UPC slab - CFT column samples (by up to 8%). The tendons significantly increased the stiffness of the samples, especially the post-cracking stiffness. The stiffness of the UPC slab - CFT column samples was 85% (when using connection T1) and 118% (when using connection T3) higher than that of the RC slab - CFT column samples.

(ii) The tendons effectively controlled the stiffness deterioration of the sample (the ratio of the post-cracking to pre-cracking stiffness). The stiffness deterioration of the UPC slab - CFT column samples was substantially smaller (2.1 times) than the RC slab - CFT column samples. This result means that on the one hand, the tendons can help control the slab deflection effectively (reducing the deflection by up to 58%) and thus ensure the serviceability requirement of the structure. On the other hand, the use of tendons embrittles the response of the slab-column connection and reduces the deformation capacity of the structure (reducing the maximum deflection by up to 51%);

(iii) The ductility index and energy absorption index of the UPC slab - CFT column samples were respectively reduced by 44% and 41% compared to the RC slab - CFT column samples. The strain of the horizontal bearing plate, the vertical rib and the rebar (by up to 75%, 81% and 91%, respectively) was also decreased when using prestressing tendons.

Acknowledgments

This research was funded by JFE Steel Corporation, Japan. The experiments were conducted at Bach Khoa Structural Engineering Laboratory of Ho Chi Minh City University of Technology (HCMUT), VNU-HCM, Vietnam. We acknowledge the support of time and facilities from Ho Chi Minh City University of Technology (HCMUT), VNU-HCM for this study.

References

[1] Corley, W. G., Hawkins, N. M. (1968). Shearhead reinforcement for slabs. *ACI Journal Proceedings*, 65 (10):811–824.

[2] Nguyen-Minh, L., Rovňák, M., Tran-Ngoc, T., Le-Phuoc, T. (2012). Punching shear resistance of post-tensioned steel fiber reinforced concrete flat plates. *Engineering Structures*, 45:324–337.

[3] Nguyen-Minh, L., Rovňák, M., Tran-Quoc, T. (2012). Punching shear capacity of interior SFRC slab-column connections. *Journal of Structural Engineering*, 138(5):613–624.

[4] Kim, J.-W., Lee, C.-H., Kang, T. H.-K. (2014). Shearhead reinforcement for concrete slab to concrete-filled tube column connections. *ACI Structural Journal*, 111(3):629–638.

[5] Lee, C.-H., Kang, T. H.-K., Kim, J.-W., Song, J.-K., Kim, S. (2019). Seismic performance of concrete-filled tube column-reinforced concrete slab connections with shear reinforcement. *ACI Structural Journal*, 116(2):233–244.

[6] Tran, D. T., Pham, T. M., Hao, H., Chen, W. (2021). Numerical investigation of flexural behaviours of precast segmental concrete beams internally post-tensioned with unbonded FRP tendons under monotonic loading. *Engineering Structures*, 249:113341.

[7] Rafiee, S., Hosseini, A., Marefat, M. S. (2021). Seismic details for exterior connections of post-tensioned flat slabs to steel columns using steel plates, vertical stiffeners and bolts. *Journal of Building Engineering*, 36:102140.

[8] Phan-Vu, P., Tran, D. T., Pham, T. M., Dang, T. D., Ngo-Huu, C., Nguyen-Minh, L. (2021). Distinguished bond behaviour of CFRP sheets in unbonded post-tensioned reinforced concrete beams versus single-lap shear tests. *Engineering Structures*, 234:111794.

[9] Tran, D. T., Pham, T. M., Hao, H., Chen, W. (2021). Numerical study on bending response of precast segmental concrete beams externally prestressed with FRP tendons. *Engineering Structures*, 241:112423.

[10] Nguyen-Minh, L., Phan-Vu, P., Tran-Thanh, D., Truong, Q. P. T., Pham, T. M., Ngo-Huu, C., Rovňák, M. (2018). Flexural-strengthening efficiency of CFRP sheets for unbonded post-tensioned concrete T-beams. *Engineering Structures*, 166:1–15.

[11] Phan-Vu, P., Tran, D. T., Ngo-Huu, C., Dang, T. D., Nguyen-Minh, L. (2018). Flexural behaviour of unbonded post-tensioned concrete t-beams strengthened with CFRP sheets under repeated loading. In *7th International Conference on Protection of Structures against Hazards (PSH2018)*, Hanoi, Vietnam: CI-Premier Pte Ltd, Singapore 238841.

[12] Truong, Q. P. T., Phan-Vu, P., Tran-Thanh, D., Dang, T. D., Nguyen-Minh, L. (2018). Flexural behavior of unbonded post-tensioned concrete T-beams externally bonded with CFRP sheets under static loading. In *Proceedings of the International Conference on Advances in Computational Mechanics 2017*, Springer Singapore, 273–289.

[13] Zhou, L., Huang, Y., Chen, B. (2021). Punching shear behavior of slab–column connections embedded with steel skeletons. *Structures*, 33:2879–2892.

[14] Yu, J. L., Wang, Y. C. (2018). Punching shear behavior and design of an innovative connection from steel tubular column to flat concrete slab. *Journal of Structural Engineering*, 144(9).

[15] Satoh, H., Shimazaki, K. (2004). Experimental research on load resistance performance of CFT column/flat plate connection. In *13th World Conference on Earthquake Engineering, Paper*, volume 976.

[16] Lee, C.-H., Kim, J.-W., Song, J.-G. (2008). Punching shear strength and post-punching behavior of CFT column to RC flat plate connections. *Journal of Constructional Steel Research*, 64(4):418–428.

[17] Yamaguchi, T., Shimazaki, K., Satou, H. (2008). An experimental study on vertical load resistance of CFT column-flat plate joints. In *Proceedings of the 14th World Conference on Earthquake Engineering, Beijing, China*.

[18] Su, Y., Tian, Y. (2009). Experimental study of RC slab-CFT column connections under seismic deformations. In *Challenges, Opportunities and Solutions in Structural Engineering and Construction*, CRC Press.

[19] Eder, M. A., Vollum, R. L., Elghazouli, A. Y. (2012). Performance of ductile RC flat slab to steel column connections under cyclic loading. *Engineering Structures*, 36:239–257.

[20] Yan, P., Wang, Y. C. (2014). Behaviour of steel tube-reinforced concrete flat slab shearhead systems. *Proceedings of the Institution of Civil Engineers - Structures and Buildings*, 167(11):667–677.

[21] Bompa, D. V., Elghazouli, A. Y. (2016). Structural performance of RC flat slabs connected to steel columns with shear heads. *Engineering Structures*, 117:161–183.

[22] Chen, C.-C., Giduquio, M. B., Chang, S.-C. L., Cheng, M.-Y. (2020). Punching shear capacity of RC slab-CFT column connections. *Engineering Structures*, 218:110785.

[23] Nguyen-Minh, L., Vo-Le, D., Tran-Thanh, D., Pham, T. M., Ho-Huu, C., Rovňák, M. (2018). Shear capacity of unbonded post-tensioned concrete T-beams strengthened with CFRP and GFRP U-wraps. *Composite Structures*, 184:1011–1029.

[24] Tran, D. T., Phan-Vu, P., Pham, T. M., Dang, T. D., Nguyen-Minh, L. (2020). Repeated and post-repeated flexural behavior of unbonded post-tensioned concrete T-beams strengthened with CFRP sheets. *Journal of Composites for Construction*, 24(2).

[25] Vo-Le, D., Tran, D. T., Pham, T. M., Ho-Huu, C., Nguyen-Minh, L. (2022). Re-evaluation of shear contribution of CFRP and GFRP sheets in concrete beams post-tensioned with unbonded tendons. *Engineering Structures*, 259:114173.

[26] Do-Dai, T., Chu-Van, T., Tran, D. T., Nassif, A. Y., Nguyen-Minh, L. (2022). Efficacy of CFRP/BFRP

laminates in flexurally strengthening of concrete beams with corroded reinforcement. *Journal of Building Engineering*, 53:104606.

[27] TCVN 10303:2014. *Concrete - Control and assessment of compressive strength*. Viet Nam Standards and Quality Institute (VSQI), Ha Noi, Vietnam.

[28] TCVN 197-1:2014. *Metallic materials - Tensile testing - Part 1: Method of test at room temperature*. Viet Nam Standards and Quality Institute (VSQI), Ha Noi, Vietnam.

[29] ACI 318-19 (2019). *Building code requirements for structural concrete*. American Concrete Institute, Farmington Hills, MI.

[30] ACI Committee 374 (2013). *Guide for testing reinforced concrete structural elements under slowly applied simulated seismic loads*. American Concrete Institute, Farmington Hills, MI.

[31] Dang, T. D., Tran, D. T., Nguyen-Minh, L., Nassif, A. Y. (2021). Shear resistant capacity of steel fibres reinforced concrete deep beams: An experimental investigation and a new prediction model. *Structures*, 33:2284–2300.

[32] Do-Dai, T., Tran, D. T., Nguyen-Minh, L. (2021). Effect of fiber amount and stirrup ratio on shear resistance of steel fiber reinforced concrete deep beams. *Journal of Science and Technology in Civil Engineering (STCE) - HUCE*, 15(2):1–13.

[33] Husain, M., Eisa, A. S., Roshdy, R. (2017). Alternatives to enhance flat slab ductility. *International Journal of Concrete Structures and Materials*, 11(1):161–169.